

# Treatment of a semi-metal to metal structural phase transition: convergence properties of the A7 $\rightarrow$ sc transition of arsenic

Patricia Silas,<sup>1</sup> Jonathan R. Yates,<sup>1</sup> and Peter D. Haynes<sup>2</sup>

<sup>1</sup>*Theory of Condensed Matter, Cavendish Laboratory, University of Cambridge, JJ Thomson Avenue, Cambridge CB3 0HE, United Kingdom*

<sup>2</sup>*Departments of Materials and Physics, Imperial College London, Exhibition Road, London SW7 2AZ, United Kingdom*

The material presented here is supplementary to the article entitled: “Density-functional investigation of the rhombohedral to simple cubic phase transition of arsenic”; it deals with the convergence issues involved in studying a semi-metal to metal structural phase transition such as the A7  $\rightarrow$  sc transition of arsenic.

The occurrence of the A7  $\rightarrow$  sc phase transition of arsenic is identified most clearly by the behavior of the nearest and next-nearest neighbor distances. In this study we investigate closely the convergence of these distances with respect to  $k$ -point grid size and smearing over the pressure ranges of 12–24 GPa and 17–30 GPa for the LDA and GGA-PBE cases, respectively. In the region of the transition, the energy differences between the two structures are extremely small. If for a given pressure the potential energy surface is noisy and rather flat, then it is possible that our system relaxes to a structure that corresponds to a local minimum, rather than the global minimum of our energy surface. We have found that to be able to achieve good results we must resolve our potential energy surface as much as possible. We have investigated Gaussian smearing,<sup>1</sup> and Methfessel-Paxton smearing,<sup>2</sup> but we find that we obtain much cleaner and clearer results by using cold-smearing<sup>3</sup> and therefore have done so throughout this study (a review of these different smearing techniques can be found in Ref. 4).

In these numerical calculations, the integrations that are to be performed over the Brillouin zone are discretized by way of the  $k$ -point grid. In the case of an insulator, no smearing is required. Smearing is only required in the event that one or more bands cross the Fermi level, in other words if the material possesses a Fermi surface (if it is a metal or a semi-metal). The effect of smearing is to blur the details of the Fermi surface (by imposing an artificial temperature on the electronic system); smearing must be used to ensure that the calculation is stable, but can also be used to hasten the convergence of the calculation. If our material does possess a Fermi surface, but we use an infinitely dense  $k$ -point grid, no smearing is needed as no details of the Fermi surface will be lost; the choice of  $k$ -point grid and smearing are coupled to each other. We would like to minimize the number of  $k$ -points used in the calculation, but must choose a grid dense enough to properly sample the Brillouin zone as well as to pick out the features of the Fermi surface. If we use a smaller (less dense)  $k$ -point grid, we must use more smearing, but the exact amount of smearing to use is not obvious. If we use a smearing that is too high, details of the Fermi surface may be washed out possibly to the extent of affecting the quantities that interest us.

It is preferable to keep the smearing low to obtain results of the highest accuracy possible, but there is a limit to how low the smearing can be set for a given  $k$ -point grid before there is a risk that the calculation becomes unstable.

In fact, to choose the smearing properly for a particular  $k$ -point grid would require knowledge of the three-dimensional band-structure of the material throughout the entire Brillouin zone, since the smearing should be determined by the steepest gradients of the bands crossing the Fermi level. (Although we cannot avoid it, it is not actually appropriate to apply a unique amount of smearing to the entire band-structure of a material undergoing a semi-metal to metal phase transition; ideally we would use some sort of adaptive smearing technique to minimize the washing-out of the features of the Fermi surface.) It is not feasible to investigate three-dimensional band-structures, so we must carefully converge our calculations with respect to both  $k$ -point grid size and smearing. Initially, we did some cursory convergence tests to determine suitable choices for the cut-off energy as well as for the density of the fine-grid, respectively to ensure an appropriate basis set size and to recover sufficient detail of the charge density within the atomic cores; these tests were performed on the uncompressed system. The results of our geometry optimizations, however, must be subjected to more rigorous convergence testing; each calculation must be repeated in its entirety for each combination of  $k$ -point grid and smearing. The properties that interest us must be converged in this way before anything can reliably be said about them. Although convergence tests for  $k$ -point grid size are standard, in electronic structure calculations that involve smearing it is very rare to find that testing has been undertaken to determine how the smearing has affected the results; yet applying a casual approach to the choice of the amount of smearing used can lead to gross inaccuracies (see Ref. 5). Thus, it is essential that tests for convergence with respect to both  $k$ -point grid and smearing be performed. Furthermore, it must be stressed that such tests should not merely be carried out by looking at what happens to the total energy of the system; rather, these tests must always be carried out on the quantities specific to the study itself.

As we mentioned above, we would like to perform an

in-depth investigation of the  $A7 \rightarrow sc$  phase transition and so we must test the convergence of our quantities of interest, the nearest and next-nearest neighbor distances, with respect to  $k$ -point grid and smearing in the region of the transition. Fig. 1 displays the results of these convergence tests for the case of the LDA. Consider first the top panel of this figure, which displays the behavior of the nearest and next-nearest neighbor distances for different grid sizes using a cold-smearing of 0.1 eV. We see that for this value of the smearing, none of the results for the different grid sizes have converged in the immediate vicinity of the transition, which appears to occur somewhere in the range of 19–21 GPa. Even our results for a  $50 \times 50 \times 50$  grid have not quite converged to those for a  $66 \times 66 \times 66$  grid. Note also how different our results at the transition are for the  $24 \times 24 \times 24$ ,  $25 \times 25 \times 25$  and  $26 \times 26 \times 26$  grids at this smearing. This is down to the particular sampling of the Brillouin zone for each specific grid and tells us that we are not using enough  $k$ -points to properly sample the Brillouin zone for this smearing and at these pressures. Outside the region of the phase transition, the calculations are less sensitive to the density of the  $k$ -point grid; below about 14 GPa and above about 30 GPa we see that our results are well converged at this smearing for all grid sizes. Hence we can be confident about our choice of grid and smearing ( $33 \times 33 \times 33$ , 0.1 eV) at pressures away from this particular transition.

If we decide that we do not require the finest features of the Fermi surface to obtain a meaningful result, then we can increase the smearing, as we have done for the middle panel of Fig. 1, for which a cold-smearing of 0.2 eV was used. We see that at this smearing, the results have converged for the three most dense grids used,  $33 \times 33 \times 33$ ,  $50 \times 50 \times 50$  and  $66 \times 66 \times 66$ , and the transition pressure seems to have shifted slightly higher appearing now to occur at 20–21 GPa.

In the lowest panel of Fig. 1, we have increased the smearing high enough to ensure that the results of all of our grids converge. Having shown, for a smearing of 0.5 eV, the convergence of the calculations for the least dense grids used, we do not repeat the calculations for the most dense grids of  $50 \times 50 \times 50$  and  $66 \times 66 \times 66$ . If we compare the top and bottom panels, we can see quite clearly that as the smearing is increased, the transition shifts to slightly higher pressures.

The components that make up the nearest and next-nearest neighbor distances are the cell angle  $\alpha$ , the atomic positional parameter  $z$ , and the lattice parameter  $a$ . We

can therefore examine the convergence properties across the transition of these constituent quantities as well. In the case of the LDA, the results of our convergence testing on  $\alpha$ ,  $z$ , and  $a$  are presented in Fig. 2, Fig. 3 and Fig. 4, respectively.

We observe similar difficulty in the convergence of the  $A7 \rightarrow sc$  phase transition in the case of the GGA-PBE. Fig. 5 shows the results in terms of the nearest and next-nearest neighbor distances of our GGA-PBE calculations for each of the same grids employed for the LDA, but for a cold-smearing of 0.1 eV only. Considering the data resulting from the use of the most dense  $k$ -point grids, we can conclude from this figure that in this case the phase transition must happen over the pressure interval of 27–29 GPa. The corresponding results of the convergence testing on  $\alpha$ ,  $z$ , and  $a$  in this case are revealed in Fig. 6, Fig. 7 and Fig. 8, respectively.

As we said above, for a cold-smearing of 0.1 eV even calculations using a  $50 \times 50 \times 50$   $k$ -point grid have not converged to those using a  $66 \times 66 \times 66$  grid in the vicinity of the transition. We can conclude just by observing the top panel of Fig. 1 that in the vicinity of the phase transition, these calculations are extremely sensitive to the details of the Fermi surface. The Fermi surface of arsenic is extremely complex. From work carried out by Lin and Falicov,<sup>6</sup> we estimate that a  $k$ -point grid at least twice as dense as our most dense grid used ( $66 \times 66 \times 66$ ) would be required to resolve all of the features of the Fermi surface of arsenic at ambient pressures.

The most dense grid employed by Da Silva, *et. al.*<sup>7</sup> in their study of arsenic was  $13 \times 13 \times 13$ , and in the case of Häussermann, *et. al.*<sup>8</sup> it was  $17 \times 17 \times 17$ . Durandurdu<sup>9</sup> uses only the gamma point for a unit cell containing 250 atoms, roughly corresponding to using a  $5 \times 5 \times 5$   $k$ -point grid for for a two-atom unit cell. Our investigations reveal that these calculations could not have been converged, and that any agreement with experiment that may have been observed in these cases was merely fortuitous.

We conclude that it is surprisingly difficult to converge the calculations for this semi-metal to metal phase transition using reasonably sized  $k$ -point grids and smearings. It is of course possible to converge the calculations using less dense grids if very large smearings are used but it would be at the expense of accuracy in the resulting transition pressures. To ensure accuracy when studying a pressure-induced semi-metal to metal phase transition, dense  $k$ -point grids are essential.

<sup>1</sup> C.-L. Fu and K.-M. Ho, Phys. Rev. B **28**, 5480 (1983).

<sup>2</sup> M. Methfessel and A. T. Paxton, Phys. Rev. B **40**, 3616 (1972).

<sup>3</sup> N. Marzari, D. Vanderbilt, A. De Vita, and M. C. Payne, Phys. Rev. Lett. **82**, 3296 (1999).

<sup>4</sup> B. G. Walker, C. Molteni, and N. Marzari, J. Phys.: Condens. Matter **16**, S2575 (2004).

<sup>5</sup> M. J. Mehl, Phys. Rev. B **61**, 1654 (2000).

<sup>6</sup> P. J. Lin and L. M. Falicov, Phys. Rev. **142**, 441 (1966).

<sup>7</sup> C. R. S. Da Silva and R. M. Wentzcovitch, Comput. Mater. Sci. **8**, 219 (1997).

<sup>8</sup> U. Häussermann, K. Söderberg, and R. Norrestam, J. Am. Chem. Soc. **124**, 15359 (2002).

<sup>9</sup> M. Durandurdu, Phys. Rev. B **72**, 073208 (2005).

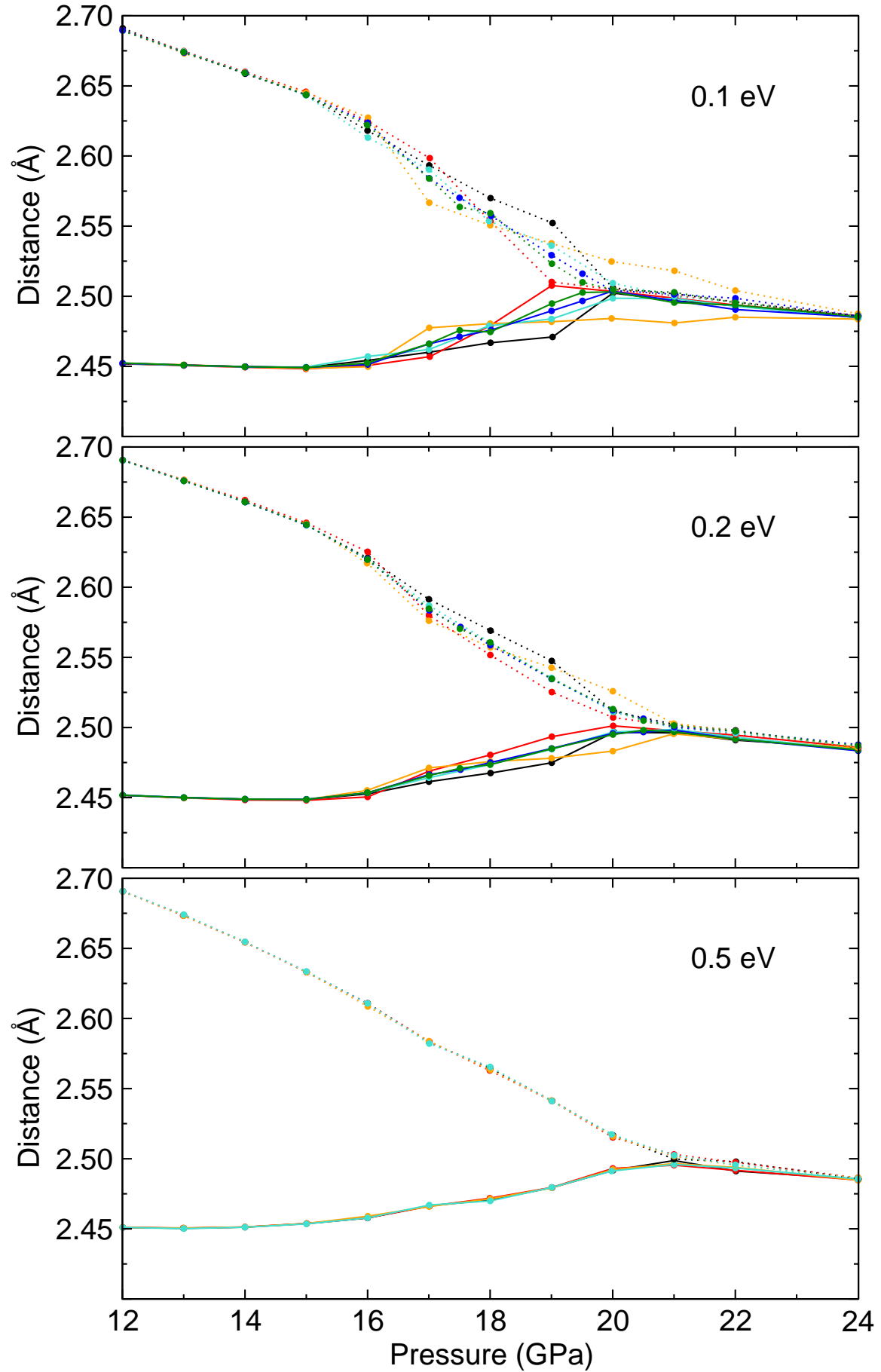


FIG. 1: Nearest neighbor (solid lines) and next-nearest neighbor (dotted lines) distances as a function of pressure for the  $A7 \rightarrow sc$  transition of arsenic using the LDA. Grids used are:  $24 \times 24 \times 24$  (black),  $25 \times 25 \times 25$  (red),  $26 \times 26 \times 26$  (orange),  $33 \times 33 \times 33$  (cyan),  $50 \times 50 \times 50$  (blue) and  $66 \times 66 \times 66$  (green). The values of cold-smearing used are: 0.1 eV (top), 0.2 eV (middle) and 0.5 eV (bottom).

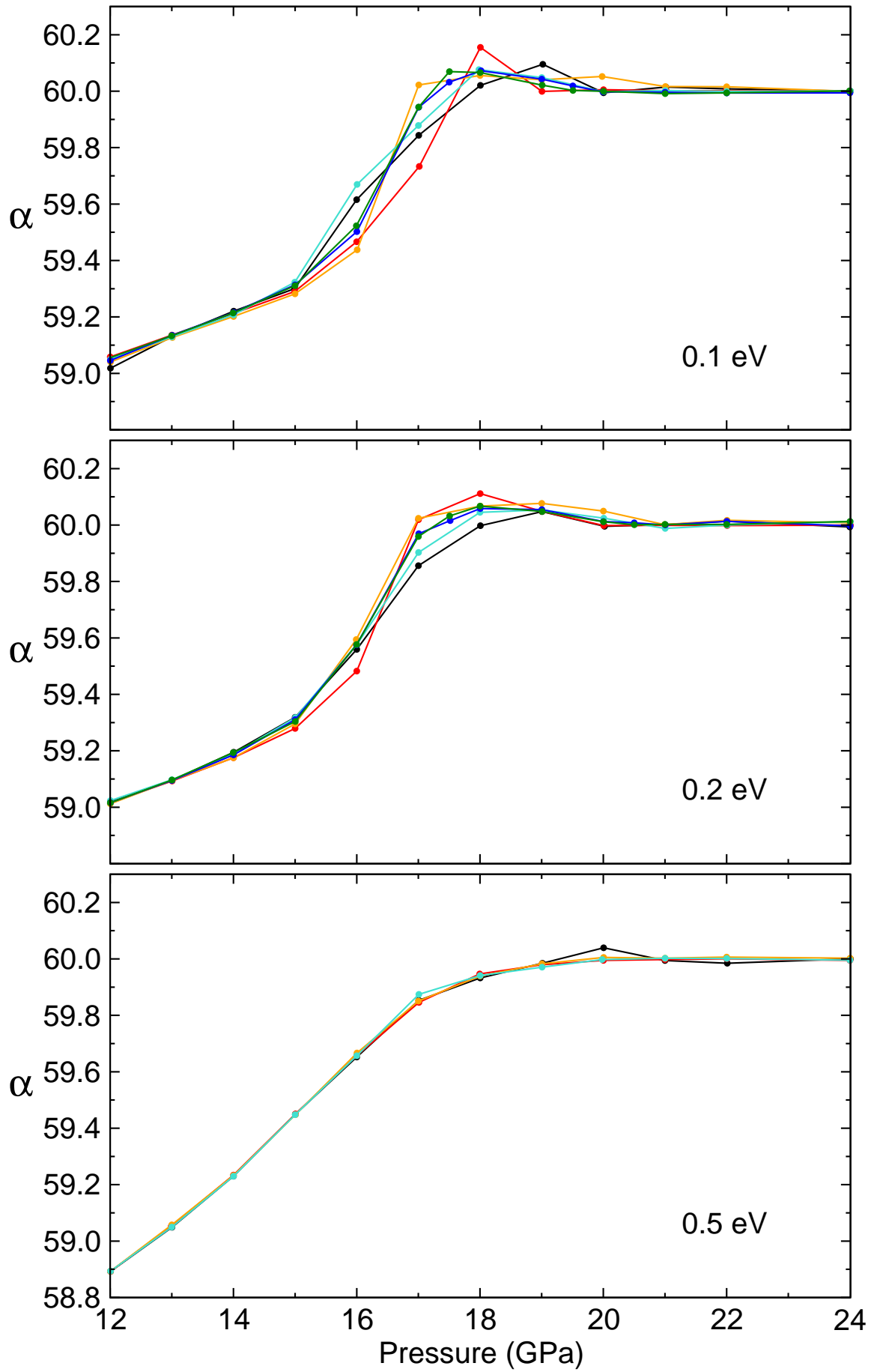


FIG. 2: Cell angle  $\alpha$  as a function of pressure for the A7  $\rightarrow$  sc transition of arsenic using the LDA. Grids used are:  $24 \times 24 \times 24$  (black),  $25 \times 25 \times 25$  (red),  $26 \times 26 \times 26$  (orange),  $33 \times 33 \times 33$  (cyan),  $50 \times 50 \times 50$  (blue) and  $66 \times 66 \times 66$  (green). The values of cold-smearing used are: 0.1 eV (top), 0.2 eV (middle) and 0.5 eV (bottom).

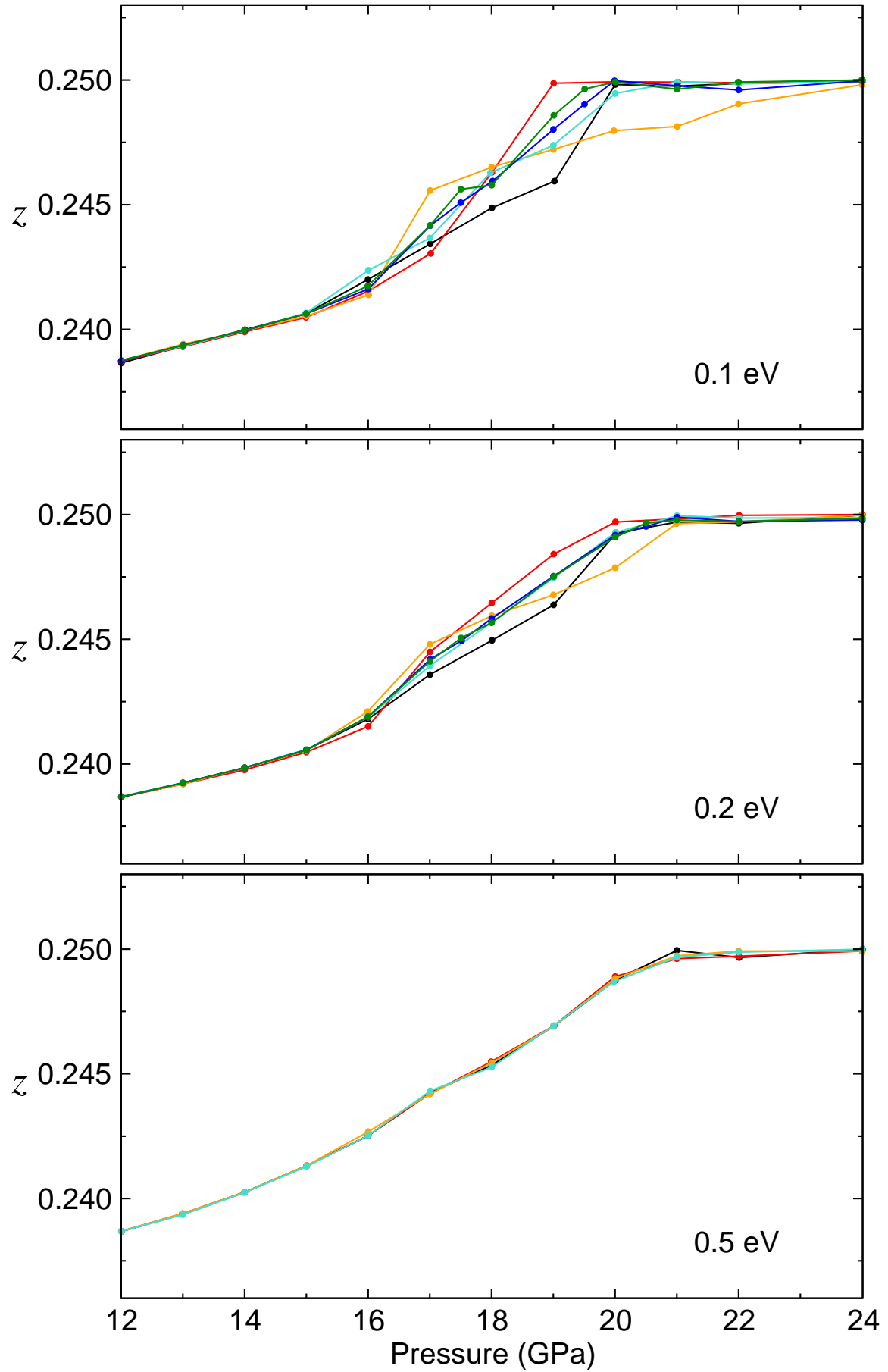


FIG. 3: Atomic positional parameter  $z$  as a function of pressure for the A7  $\rightarrow$  sc transition of arsenic using the LDA. Grids used are: 24×24×24 (black), 25×25×25 (red), 26×26×26 (orange), 33×33×33 (cyan), 50×50×50 (blue) and 66×66×66 (green). The values of cold-smearing used are: 0.1 eV (top), 0.2 eV (middle) and 0.5 eV (bottom).

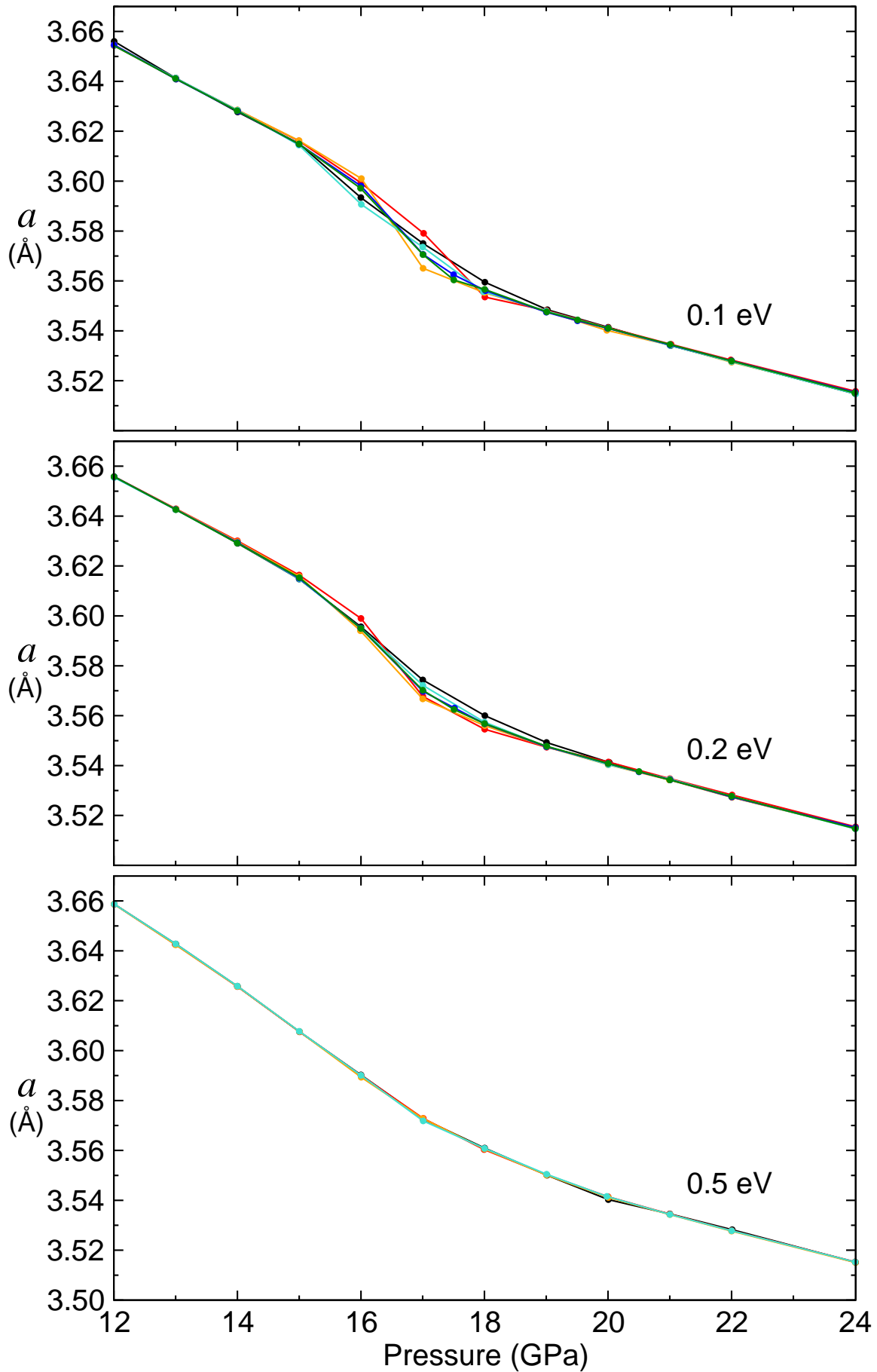


FIG. 4: Lattice parameter  $a$  as a function of pressure for the A7  $\rightarrow$  sc transition of arsenic using the LDA. Grids used are:  $24 \times 24 \times 24$  (black),  $25 \times 25 \times 25$  (red),  $26 \times 26 \times 26$  (orange),  $33 \times 33 \times 33$  (cyan),  $50 \times 50 \times 50$  (blue) and  $66 \times 66 \times 66$  (green). The values of cold-smearing used are: 0.1 eV (top), 0.2 eV (middle) and 0.5 eV (bottom).

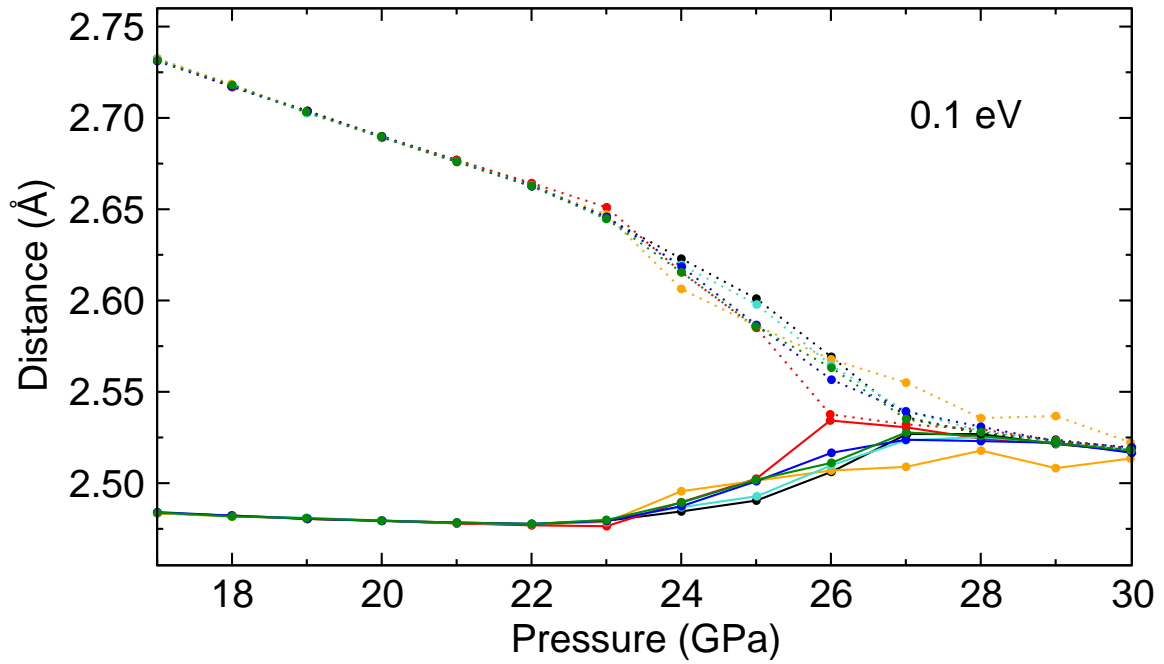


FIG. 5: Nearest neighbor (solid lines) and next-nearest neighbor (dotted lines) distances as a function of pressure for the  $A7 \rightarrow sc$  transition of arsenic using the GGA-PBE. Grids used are:  $24 \times 24 \times 24$  (black),  $25 \times 25 \times 25$  (red),  $26 \times 26 \times 26$  (orange),  $33 \times 33 \times 33$  (cyan),  $50 \times 50 \times 50$  (blue) and  $66 \times 66 \times 66$  (green), each with a cold-smearing of 0.1 eV.

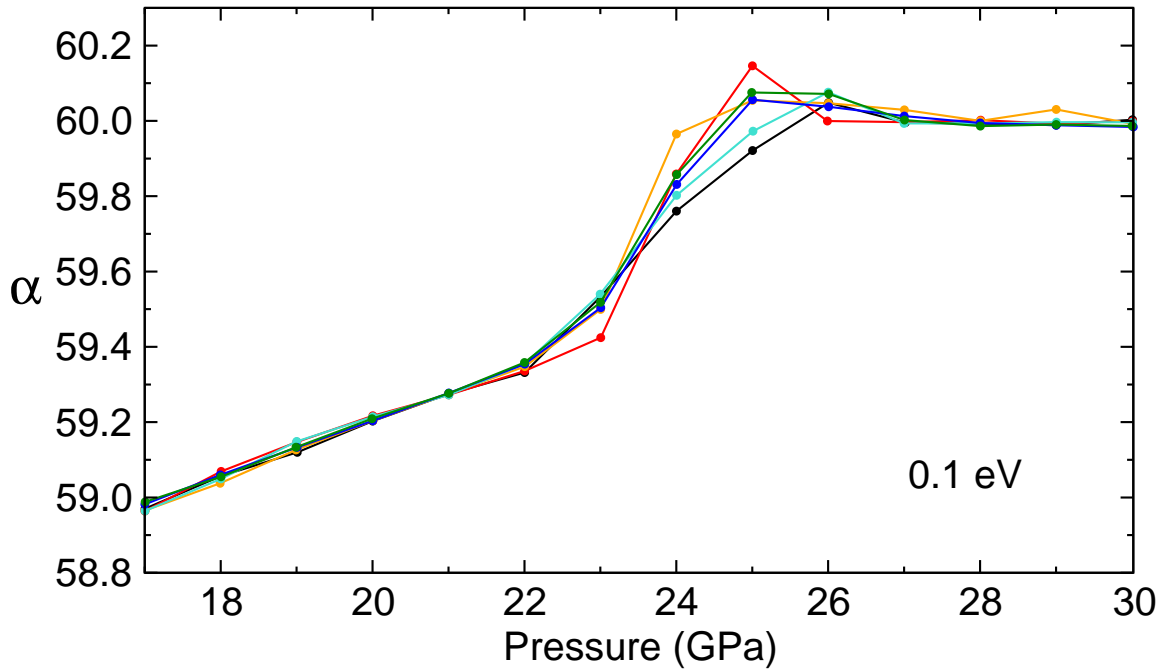


FIG. 6: Cell angle  $\alpha$  as a function of pressure for the  $A7 \rightarrow sc$  transition of arsenic using the GGA-PBE. Grids used are:  $24 \times 24 \times 24$  (black),  $25 \times 25 \times 25$  (red),  $26 \times 26 \times 26$  (orange),  $33 \times 33 \times 33$  (cyan),  $50 \times 50 \times 50$  (blue) and  $66 \times 66 \times 66$  (green), each with a cold-smearing of 0.1 eV.

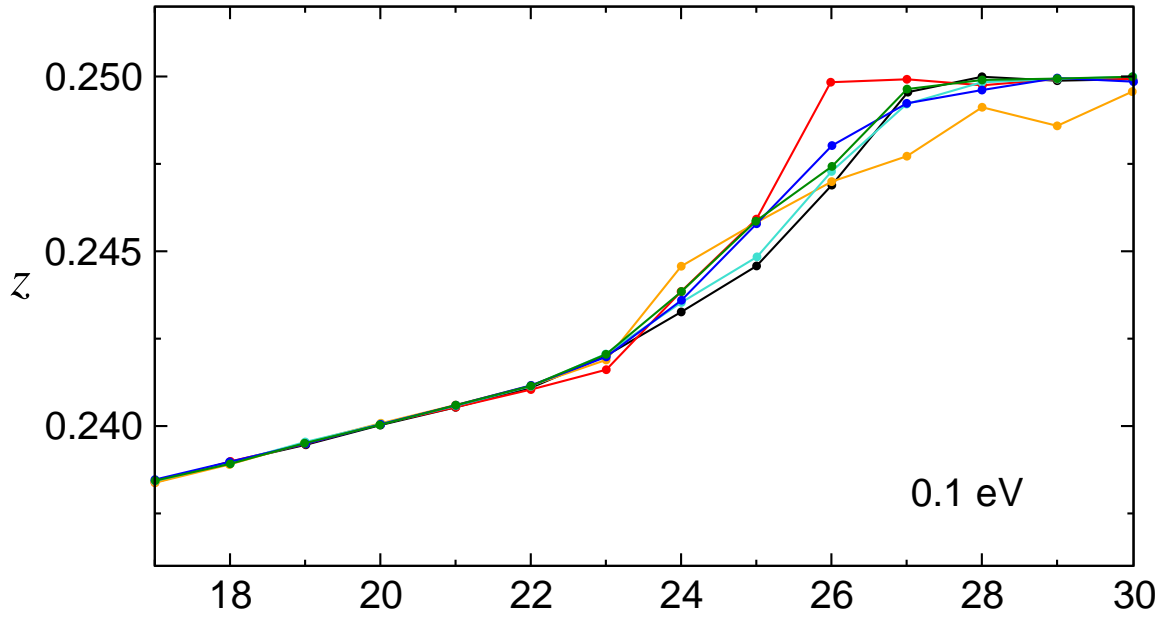


FIG. 7: Atomic positional parameter  $z$  as a function of pressure for the A7  $\rightarrow$  sc transition of arsenic using the GGA-PBE. Grids used are:  $24 \times 24 \times 24$  (black),  $25 \times 25 \times 25$  (red),  $26 \times 26 \times 26$  (orange),  $33 \times 33 \times 33$  (cyan),  $50 \times 50 \times 50$  (blue) and  $66 \times 66 \times 66$  (green), each with a cold-smearing of 0.1 eV.

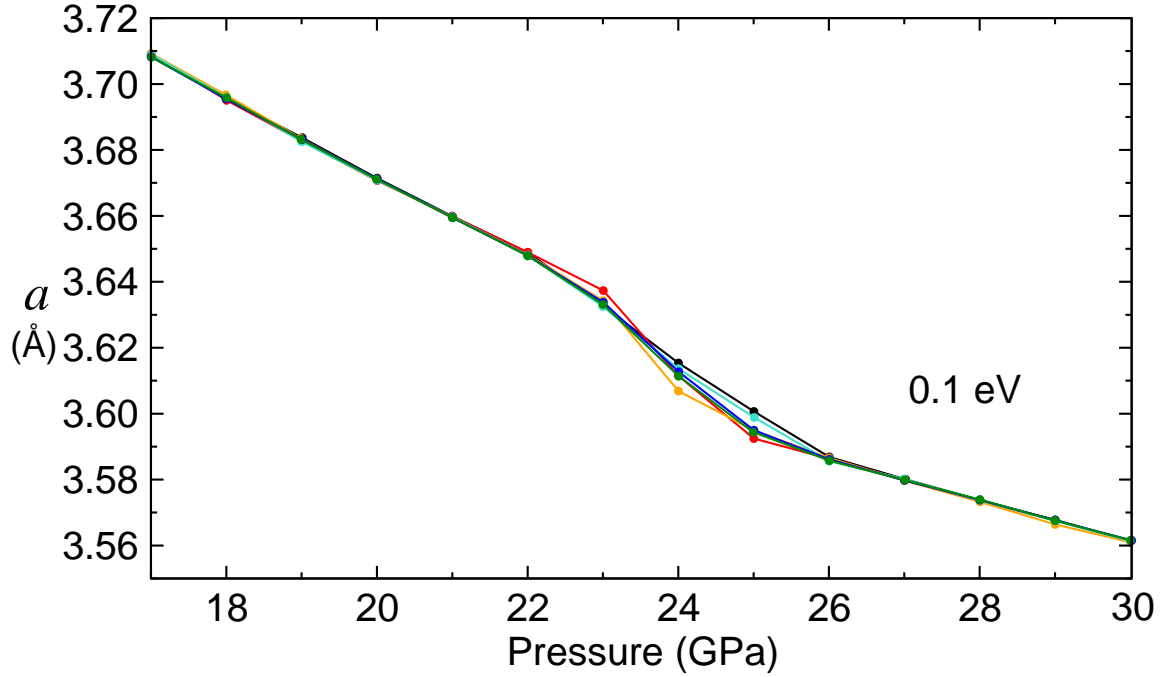


FIG. 8: Lattice parameter  $a$  as a function of pressure for the A7  $\rightarrow$  sc transition of arsenic using the GGA-PBE. Grids used are:  $24 \times 24 \times 24$  (black),  $25 \times 25 \times 25$  (red),  $26 \times 26 \times 26$  (orange),  $33 \times 33 \times 33$  (cyan),  $50 \times 50 \times 50$  (blue) and  $66 \times 66 \times 66$  (green), each with a cold-smearing of 0.1 eV.